

UKAEA-CCFE-PR(22)44

D. Power, S. Mijin, F. Militello, R. Kingham

Scaling laws for electron kinetic effects in tokamak scrape-off layer plasmas

Enquiries about copyright and reproduction should in the first instance be addressed to the UKAEA Publications Officer, Culham Science Centre, Building K1/O/83 Abingdon, Oxfordshire, OX14 3DB, UK. The United Kingdom Atomic Energy Authority is the copyright holder.

The contents of this document and all other UKAEA Preprints, Reports and Conference Papers are available to view online free at scientific-publications.ukaea.uk/

Scaling laws for electron kinetic effects in tokamak scrape-off layer plasmas

D. Power, S. Mijin, F. Militello, R. Kingham

Scaling laws for electron kinetic effects in tokamak scrape-off layer plasmas

D Power¹ S Mijin² F Militello² R Kingham¹

¹Blackett Lab., Plasma Physics Group, Imperial College London,
London SW7 2AZ, United Kingdom

²UKAEA, Culham Science Centre, Abingdon, Oxon OX14 3DB,
United Kingdom

August 22, 2022

Abstract

Tokamak edge (scrape-off layer) plasmas can exhibit non-local transport in the direction parallel to the magnetic field due to steep temperature gradients. This effect along with its consequences has been explored at equilibrium for a range of conditions, from sheath-limited to detached, using the 1D kinetic electron code SOL-KiT, where the electrons are treated kinetically and compared to a self-consistent fluid model. Line-averaged suppression of the kinetic heat flux (compared to Spitzer-Härm) of up to 48% is observed, contrasting with up to 57% enhancement of the sheath heat transmission coefficient, γ_e . Simple scaling laws in terms of basic SOL parameters for both effects are presented. By implementing these scalings as corrections to the fluid model, we find good agreement with the kinetic model for target electron temperatures. It is found that the strongest kinetic effects in γ_e are observed at low-intermediate collisionalities, and tend to increase at increasing upstream densities and temperatures. On the other hand, the heat flux suppression is found to increase monotonically as upstream collisionality decreases. The conditions simulated include regimes relevant to current and future tokamaks.

1 Introduction

The region of unconfined plasma at the edge of tokamaks, called the scrape-off layer (SOL), is the barrier between the hot core plasma and the solid surfaces which make up the inside of the reactor. It is necessary to understand plasma transport in this region, which occurs primarily parallel to the magnetic field lines, so that accurate predictions can be made for future devices and steps can be taken to mitigate heat fluxes which may exceed material constraints.

Transport in SOL plasmas is often treated with fluid models, where a Braginskii-like set of transport equations [1] may be solved. However, the presence of steep temperature gradients parallel to the magnetic field, as would be expected in reactor-class devices, means heat transport (particularly for the electrons) may be dominated by fast, low-collisionality particles and so becomes ‘non-local’. This can be quantified with the upstream collisionality parameter $\nu_u^* = L/\lambda_u$ [2], defined as the ratio of the parallel SOL length L and the upstream mean free path λ_u . Conditions where ν_u^* is small and temperature gradients are large may not be described accurately by a fluid model.

This effect has been explored in recent years [3–11], where it is now well-documented that kinetic suppression of the heat flux can result in steeper temperature gradients and lower target temperatures when compared to a fluid model. Somewhat less understood is the region of operating parameter space where such effects may become important, and the consequences for the overall energy balance at equilibrium (i.e. how energy going into the SOL makes its way out). It is still unclear whether kinetic effects in parallel transport pose a significant uncertainty in modelling approaches for future devices.

Here we present kinetic and fluid simulations of a 1D SOL plasma model, across a wide range of the relevant parameter space (input power and plasma density), in order to assess and understand kinetic deviations from fluid model predictions. The model will briefly be presented in Section 2, followed by an explanation of the simulations that have been carried out in Section 3. We will then summarise the results (Section 4), highlighting the areas in which kinetic effects are (and are not) seen. Following a discussion of the observed results (Section 5), we present scaling relationships in terms of basic SOL parameters for the main kinetic effects seen - enhancement to the sheath heat transmission coefficient and suppression of the parallel heat flux - in Section 6. These will be used to reproduce electron temperature profiles from kinetic simulations in a (corrected) fluid model.

2 Kinetic and fluid modelling with SOL-KiT

SOL-KiT is a fully implicit 1D plasma code which has been used to study kinetic effects in parallel electron transport in the SOL [3, 12, 13]. Here a very brief outline of SOL-KiT is presented, and the reader is referred to [14] for more details of the model.

In kinetic mode, SOL-KiT solves the VFP equation for electrons in a hydrogenic plasma along the direction parallel to the magnetic field (the x -axis),

$$\frac{\partial f(x, \vec{v}, t)}{\partial t} + v_x \frac{\partial f(x, \vec{v}, t)}{\partial x} - \frac{e}{m_e} E \frac{\partial f(x, \vec{v}, t)}{\partial v_x} = \sum_{\alpha} C_{e-\alpha}, \quad (1)$$

where $f(x, \vec{v}, t)$ is the electron velocity distribution, which is a function of space, velocity and time. E is the electric field along x , m_e is the electron mass, e is the electron charge and v_x is the electron velocity along x . The right hand side consists of Fokker-Planck collisions (electron-electron and electron-ion) and Boltzmann collisions (electron-neutral). A spherical harmonic decomposition in velocity space is used to solve this equation as outlined in [15]. Azimuthal symmetry is assumed about the x -axis so that the magnetic field may be ignored.

The x -axis spans from the midplane at $x = 0$ ('upstream'), to the plasma sheath boundary at $x = L$, where L is the domain length, which is half the connection length (the parallel distance between two strike points in a divertor SOL). Power enters the plasma upstream, and leaves at the sheath or through plasma-neutral collisions. The included collisional processes are electron-impact ionisation and excitation; the inverse of these processes (three-body recombination and collisional de-excitation); and resonant charge exchange (CX) between the ions and neutrals. In addition, radiative recombination and de-excitation are modelled, which allows energy to leave the plasma-neutral system.

In fluid mode, moments of equation (1) are solved instead, allowing for a direct comparison between a fluid and kinetic treatment. Evolution equations for the electron temperature T_e , flow velocity u_e and density n_e are solved. The T_e equation is closed with Braginskii/Spitzer-Härm heat flow [1, 16], $q_{\parallel, e} = -\kappa_e \frac{\partial(kT_e)}{\partial x} + 0.71n_e kT_e (u_e - u_i)$.

Quasi-neutrality is enforced by setting the ion density $n_i = n_e$. The parallel electric field E is evolved with Ampère-Maxwell's law, $\frac{\partial E}{\partial t} = -(j_e - j_i)/\epsilon_0$, where the ion and electron currents are $j_{i, e} = \pm n_{i, e} u_{i, e}$. The implicit time integration used by SOL-KiT means this results in ambipolarity when using timesteps large relative to the plasma oscillation period.

In kinetic mode, where fluid electron quantities are required, for example u_e in calculating E , the appropriate velocity moments of f are taken.

In order to provide a realistic background on which to solve electron transport, SOL-KiT also models the hydrogenic ions and neutral atoms, both of which are treated with fluid models (discussed more in the next section). Atomic processes including ionisation, recombination, excitation and de-excitation are handled by solving a collisional-radiative model (CRM) for the neutral atoms alongside the transport equations, using fundamental cross-sections and rates from Janev [17] and NIST [18]. The fully time-dependent CRM coupled with neutral transport gives a non-coronal model. Particle sources and the effect of electron-neutral collisions on the electrons are evaluated with the inelastic Boltzmann collision operator. In fluid mode, the kinetic collision operators are evaluated with a Maxwellian electron distribution. At present no impurity species are treated by SOL-KiT, although this is planned for a future update to the code.

The upstream boundary is reflective. At the sheath boundary, the Bohm criterion is applied so that plasma flow reaches the sound speed c_s . All plasma particle flux across this boundary is lost and recycled as atomic neutrals, which are placed in the

last spatial cell. In kinetic mode, the logical boundary condition [19] is applied to the electron distribution, where the forward-going part of the distribution is reflected and truncated at some velocity v_c , which is calculated iteratively to ensure equal electron and ion fluxes. In fluid mode, this same boundary condition manifests via the heat flux at the sheath entrance, $q_{sh,e} = \gamma_e k T_{e,t} \Gamma_t$, for target temperature $T_{e,t}$ and particle flux Γ_t , and where

$$\gamma_e = 2 - 0.5 \ln(2\pi (1 + T_{i,t}/T_{e,t}) m_e/m_i) \quad (2)$$

is the sheath heat transmission coefficient [2].

2.1 Extensions to SOL-KiT

For this study, this SOL-KiT model described in [14] has been extended to provide a more realistic background plasma on which to solve the electron transport, as well to provide some reduction in compute time. As some of these improvements have not yet been documented elsewhere, they are outlined briefly here.

Firstly, an ion temperature equation has been added to the model, allowing for ion energy transport independently from the electrons as well as additional channels for ion-electron and ion-neutral energy transfer. More detail on this change is provided in [13], omitted here for brevity. The ion heat flow is $q_{\parallel,i} = -\kappa_i \frac{\partial(kT_i)}{\partial x}$, using the Spitzer-Härm κ_i [16]. The sheath boundary condition on the ion temperature equation is equivalent to the one for the fluid electron model, $q_{sh,i} = \gamma_i k T_{i,t} \Gamma_t$, with $\gamma_i = 2.5$. In fluid mode, ion-electron energy transfer is treated with $Q_{ie} = -Q_{ei} = -\frac{3m_e}{m_i} \frac{n_e k}{\tau_e} (T_i - T_e)$ [1], where τ_e is the electron collision time. In kinetic mode, we instead take the energy moment of the Fokker-Planck collision operator assuming Maxwellian ions, $Q_{ei} = \int \frac{1}{2} m_e v^2 C_{ei} d\vec{v}$. The two approaches are equivalent for Maxwellian electrons [13].

Secondly, velocity and temperature equations have been added for the (hydrogenic) neutral particles, in order to capture the important processes of energy and momentum transfer between ions and neutrals via particle exchange from ionisation, recombination and CX. This neutral model is broadly similar to that used in the SD1D code [20]. We solve for the parallel neutral velocity $u_{n,\parallel}$, with mass equal to the ion mass $m_n = m_i$,

$$\frac{\partial u_{n,\parallel}}{\partial t} = -u_{n,eff} \frac{\partial u_{n,\parallel}}{\partial x} - \frac{1}{m_n n_n} \frac{\partial p_n}{\partial x} - \frac{S_n}{n_n} u_{n,\parallel} + \frac{1}{m_n n_n} R_{n,\parallel}, \quad (3)$$

as well as the perpendicular velocity $u_{n,\perp}$ (required because we cannot assume neutral transport is primarily along the magnetic field),

$$\frac{\partial u_{n,\perp}}{\partial t} = -u_{n,eff} \frac{\partial u_{n,\perp}}{\partial x} - \frac{1}{m_n n_n \tan \alpha} \frac{\partial p_n}{\partial x} - \frac{S_n}{n_n} u_{n,\perp} + \frac{1}{m_n n_n} R_{n,\perp}, \quad (4)$$

where $p_n = n_n k T_n$ is the neutral pressure, S_n is the neutral particle source and $R_{n,\parallel}$, $R_{n,\perp}$ are the parallel and perpendicular momentum sources. Here, α is the pitch angle of the magnetic field lines relative to the wall, where $\alpha = 90^\circ$ means normal incidence. This parameter in practice determines the degree to which neutrals are

able to transport upstream in this 1D model. The effective parallel neutral velocity is $u_{n,eff} = u_{\parallel} + \frac{u_{\perp}}{\tan \alpha}$. For calculating $R_{n,\perp}$, the plasma is assumed to be stationary in the perpendicular direction. If we drop all but the pressure gradient and friction terms in (4), we recover the pressure-diffusion model [21]. This simplification has been adopted for the studies presented in this paper.

SOL-KiT solves a continuity equation for each excited state of a neutral hydrogenic species, denoted with subscript b , each with its own density n_b and particle source S_b . Total neutral density is therefore $n_n = \sum_b n_b$, and $S_n = \sum_b S_b$. The additional velocity equations (3 & 4) yields a modified continuity equation for each species,

$$\frac{\partial n_b}{\partial t} = -\frac{\partial (n_b u_{n,eff})}{\partial x} + S_b. \quad (5)$$

The neutral temperature T_n is also evolved,

$$\begin{aligned} \frac{\partial kT_n}{\partial t} = & -u_{n,eff} \frac{\partial T_n}{\partial x} \\ & + \frac{2}{3} \left[\frac{Q_n}{n_n} - kT_n \frac{\partial u_{n\parallel}}{\partial x} - \frac{S_n}{n_n} \left(\frac{3}{2} kT_n - \frac{1}{2} m_n u_{n\parallel}^2 \right) - \frac{1}{n_n (1 + \tan^2 \alpha)} \frac{\partial q_n}{\partial x} - \frac{u_{n\parallel} R_{n\parallel}}{n_n} \right], \end{aligned} \quad (6)$$

where q_n is the neutral heat flow, $q_n = -2.4 \left(\frac{n_n T_n}{m_n \nu_{CX}} \right) \frac{\partial T_n}{\partial x}$ [22] and ν_{CX} is the CX collision frequency. The energy source term Q_n contains contributions from CX collisions and the energy transfer from particle exchange during ionisation and recombination. Recycled neutrals are introduced at 3eV with no net momentum. The boundary condition on (6) is similar to the plasma species, $q_{sh,n} = \gamma_n kT_{n,t} n_{n,t} v_{th,n}$ where $v_{th,n}$ is the neutral thermal velocity. While the neutrals do not directly experience the sheath, this expression captures the effect of incident neutrals reflecting back with less energy due to surface effects. We approximate this with $\gamma_n = 0.25$.

The final change is to introduce bundling on the neutral states, so that a reduced number of states are evolved without significantly altering the plasma-neutral physics. This is desirable as it reduces the number of electron-neutral collision operators in (1) which need to be computed, which increases with the square of the number of evolved neutral states and therefore represents a code bottleneck.

We evolve all states from $b = 1$ to $\tilde{b} - 1$ as normal, and group all higher states (from \tilde{b} to $b_{max} = 30$) into a single bundle β , with bundle density $n_\beta = \sum_{b \in \beta} n_b$. Note that \tilde{b} is an optional parameter. For this bundle, we assume a Boltzmann state distribution at the electron temperature, giving the density ratio $n_b/n_{\tilde{b}} = (b/\tilde{b})^2 e^{-(\varepsilon_{\tilde{b}} - \varepsilon_b)/kT_e}$ for $b \geq \tilde{b}$, where ε_b is the ionisation energy of level b , which for hydrogen is $\varepsilon_b = 13.6\text{eV}/b^2$.

All particle, momentum and energy source terms relating to this bundle can then be computed by evaluating the appropriate collision operator with bundle-averaged cross-sections, $\langle \sigma \rangle_\beta$ and ionisation energies, $\langle \varepsilon \rangle_\beta$. These quantities are functions of the electron temperature, and are precomputed on a relevant range of T_e and interpolated at runtime. For example, the electron energy sink from ionisation of neutrals in β is

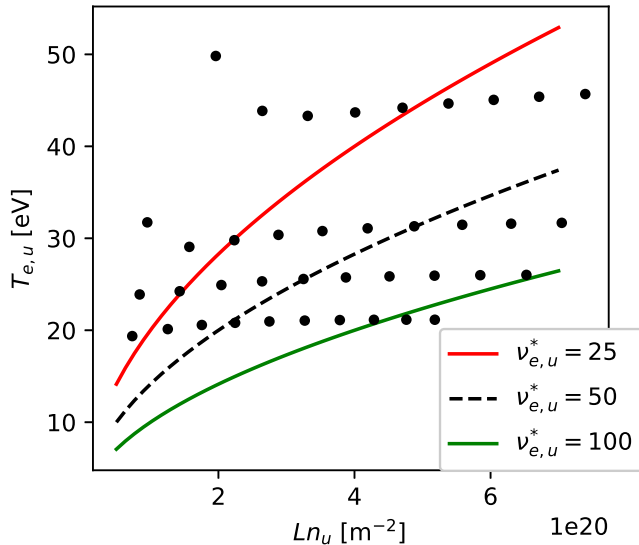


Figure 1: SOL-KiT simulations carried out for this study, where each black dot represents a pair of kinetic/fluid simulations at a given q_{in} and $\langle n \rangle$. The exact values of n_u and $T_{e,u}$ are taken from the kinetic simulations. For context, lines of constant collisionality are shown at $\nu_{e,u}^* = 25, 50$ and 100 .

$$\begin{aligned}
 Q_{\beta}^{ion} &= \langle \varepsilon \rangle_{\beta} S_{\beta}^{ion} \\
 &= \langle \varepsilon \rangle_{\beta} n_{\beta} n_e \langle K \rangle_{\beta}^{ion} \\
 &= \langle \varepsilon \rangle_{\beta} n_{\beta} n_e 4\pi \int_{\infty} dv v^3 \frac{f_0(v)}{n_e} \langle \sigma \rangle_{\beta}^{ion},
 \end{aligned} \tag{7}$$

where S_{β}^{ion} is the ionisation particle source from β , $\langle K \rangle_{\beta}^{ion}$ is the bundle-averaged ionisation rate coefficient, n_e is the electron density and f_0 is the isotropic part of the electron distribution. We also include an effective collision operator to capture excitation collisions within a bundle by assuming the net excitation rate is equal to the rate of radiative de-excitation.

Using $\tilde{b} = 5$, this bundling method is found to predict neutral densities and radiative losses to within a few percent of that predicted by directly evolving all states, while providing a factor 5-10 reduction in compute time. Further details of this bundling approach will be published separately.

3 Parameter scan simulations

Two SOL parameters which we have some degree of control over in tokamaks (and which determine SOL behaviour) are T_u and n_u , the plasma temperature and density measured at some upstream location. In these simulations, we vary these by changing the input power flux to the SOL from the core, q_{in} , and the initial line-averaged plasma density, $\langle n \rangle$ (where the plasma is fully ionised at initialisation). Of interest in this study is how conditions upstream determine the electron transport,

and a useful measure of this is the electron upstream collisionality parameter $\nu_{e,u}^*$, defined as the ratio of the connection length L to the electron Coulomb mean free path upstream $\lambda_{ee,u}$ [2],

$$\nu_{e,u}^* = \frac{L}{\lambda_{ee,u}} \simeq 10^{-16} \frac{Ln_u}{T_{e,u}^2}$$

for $T_{e,u}$ in [eV] and n_u in [m^{-3}]. Note that this differs slightly from some forms of $\nu^* = L/\lambda_u$ employed in the literature (e.g. [4]), and $\nu_{e,u}^*$ here will typically be smaller than collisionality defined in terms of total plasma temperature because $T_{i,u} > T_{e,u}$ generally.

For a deuterium plasma, a total of 78 equilibrium simulations have been done (39 fluid and 39 kinetic), which can be grouped into four density scans, with $\langle n \rangle$ ranging from 10^{19} to 10^{20}m^{-3} at $q_{in} = 4, 8, 16$ and 64MWm^{-2} . The connection length is $L = 11.64 \text{m}$ for all simulations. With these input parameters, the simulations cover $\nu_{e,u}^*$ from 8 to 114. At the lowest collisionalities the plasma is sheath-limited, while detachment is reached at the highest values of $\nu_{e,u}^*$ (measured by rollover of the target particle flux).

q_{in} is distributed over the first 3.96m of the domain and spread equally between the ions and electrons; 100% of plasma particles lost to the sheath are recycled as neutrals; and the pitch angle used in the neutral model was $\alpha = 15^\circ$. 100 spatial cells were used, which were spaced logarithmically with higher resolution close to the target. Spatial grid widths ranged from 0.57m to 4.2mm. In velocity space (for kinetic electron runs), a geometric grid of 80 cells was used up to a velocity of $\simeq 12v_{th,0}$, where $v_{th,0}$ is the thermal velocity of electrons at a reference temperature of 10eV. The resolution was higher at low velocities, such that grid widths ranged from $0.05v_{th,0}$ to $0.35v_{th,0}$. In the kinetic runs, the kinetic equation (1) was solved up to the spherical harmonic $l_{max} = 3$.

To reach equilibrium, determined by when the power and particle balance has converged, the kinetic simulations with SOL-KiT each take a few weeks running on 16 CPUs, while the fluid simulations typically take a day or two on 4 CPUs.

These simulations are situated on the $T_{e,u}$ - Ln_u plane along with lines of constant $\nu_{e,u}^*$ in Figure 1. For reference, present-day tokamaks (JET, DIII-D, etc.) operate with $Ln_u \simeq 10^{20} - 10^{21} \text{m}^{-2}$ and $T_{e,u} \simeq 20 - 60 \text{eV}$. Future devices like ITER and DEMO will operate with several times these values. Simulating such regimes kinetically is computationally demanding, but the intention of this study is to understand how parallel transport changes as upstream conditions are varied, and this is not expected to change fundamentally in larger devices. In Section 6 we will discuss an additional density scan with increased L and q_{in} to test whether an observed relationship in kinetic effects holds at these more reactor-relevant conditions.

4 Results

We start by displaying in Figure 2 the target temperatures and particle fluxes of the simulations carried out, divided into four density scans at a constant input power. Rollover of the target flux, an indicator of detachment onset, is expected when particle, momentum and power losses are sufficient to reduce the target flux

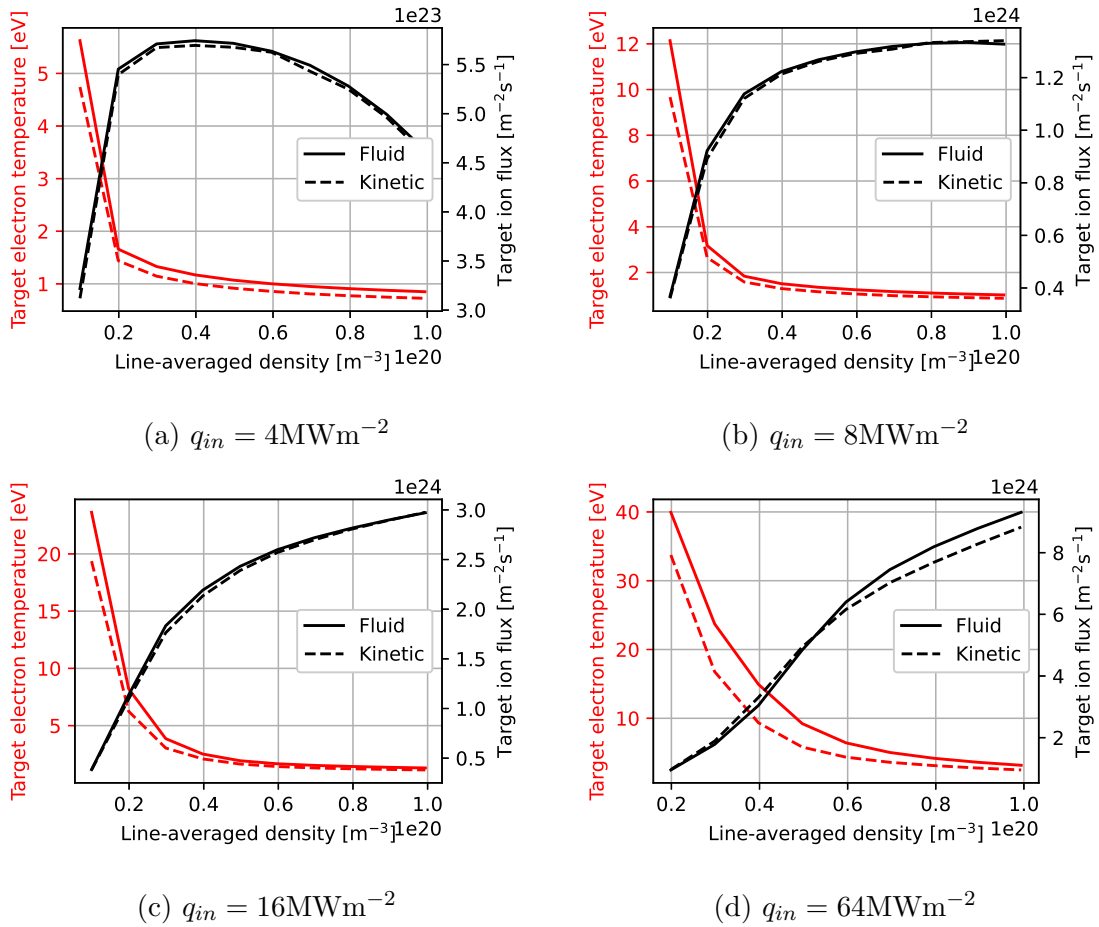


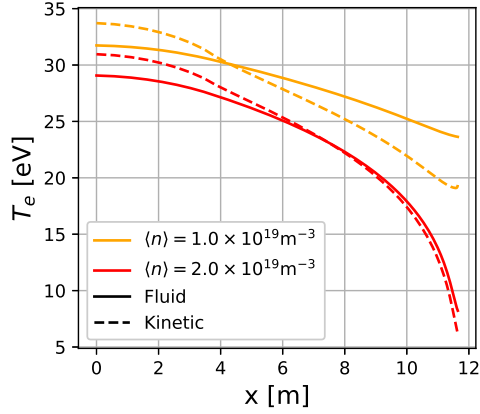
Figure 2: Target temperatures and ion fluxes for each density scan, shown for both fluid and kinetic electrons.

despite increasing plasma density. It can be seen that only the lowest-power run reaches flux rollover within this density range¹. This is not unexpected given the lack of impurity radiation in the SOL-KiT model, which would lead to rollover at higher input powers. A second feature of these target flux plots is that, while there is a modest decrease in target temperatures for kinetic electrons at low densities, the target flux profiles are broadly unchanged. As will be discussed, this is despite some significant differences between the kinetic and fluid simulations.

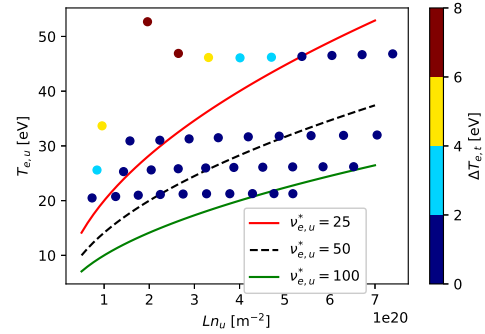
The reduction in target temperatures in Figure 2 is a reflection of the heat flux suppression which is observed in kinetic simulations, as has been observed in other kinetic studies of parallel transport [6, 7, 12, 23]. This can be seen in Figure 3a, which shows temperature profiles for two simulations at moderately low collisionality, along with differences in target electron temperatures across all simulations in Figure 3b. Figure 3c shows the ratio of the kinetic to Spitzer-Härm heat flux calculated on the kinetic plasma profiles in 3a. This suppression of the heat flux relative to that

¹This is in contrast to the flux rollover observed at $\langle n \rangle \simeq 3 \times 10^{19} \text{m}^{-3}$ in the study by Dudson et al. in [20], which uses a similar simulation setup for the SD1D code with $q_{in} = 50 \text{MWm}^{-2}$. A separate investigation has highlighted that an overestimation of the ionisation rate in SD1D is the primary reason for this difference.

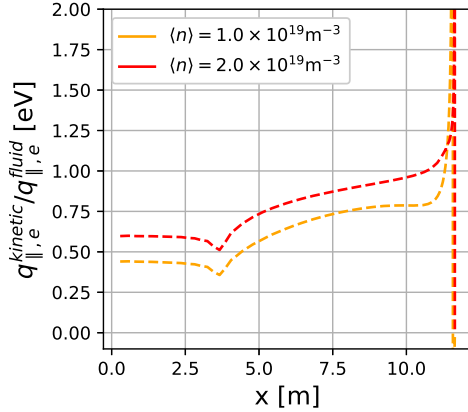
predicted by a fluid treatment, where for a given heat conductivity κ the heat flux is $q_{\parallel,e} = -\kappa\nabla T$, arises due to fast electrons not depositing their energy locally due to their large mean free path relative to the temperature gradient length scale. This means that a steeper temperature gradient is required to achieve the same heat flux along the SOL, which is fixed by q_{in} . This is also reflected in the sharp peak in the heat flux ratio close to the wall in Figure 3c, which reflects the accumulation of fast electrons there from upstream. This can also be seen in Figure 4, where an electron energy distribution close to the target is shown. There is a clear enhanced high-energy tail, while the thermal bulk is close to the local Maxwellian.



(a) Fluid and kinetic electron temperature profiles ($q_{in} = 16\text{MWm}^{-2}$).



(b) Difference in target electron temperature, $\Delta T_{e,t} = T_{e,t}^{fluid} - T_{e,t}^{kinetic}$ for each pair of fluid and kinetic simulations at a given q_{in} and $\langle n \rangle$



(c) Ratio of the kinetic to Spitzer-Härm conductive heat flux for the kinetic simulations in (a).

Figure 3: Kinetic heat flux suppression resulting in steeper temperature gradients and lower target temperatures for two low collisionality simulations ($q_{in} = 16\text{MWm}^{-2}$).

In Figure 5, we show the kinetic enhancement of the sheath heat transmission coefficient γ_e , shown separately for each group of simulations at fixed q_{in} (5a), and for all simulations on the $T_{e,u}-Ln_u$ plane (5b). Differences in γ_e here arise because,

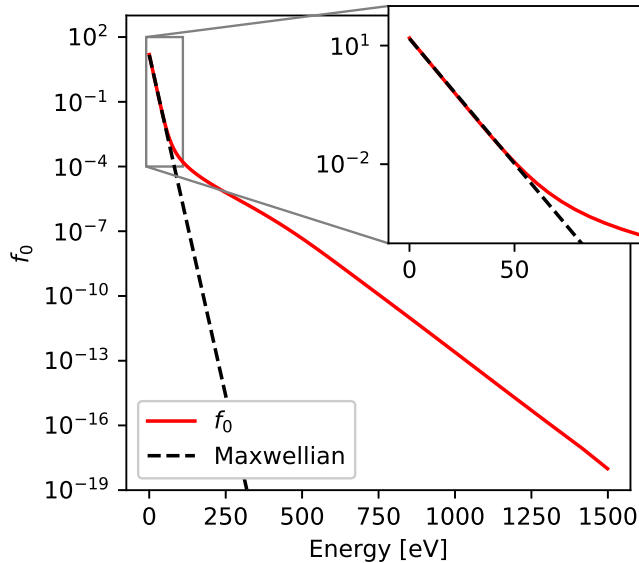
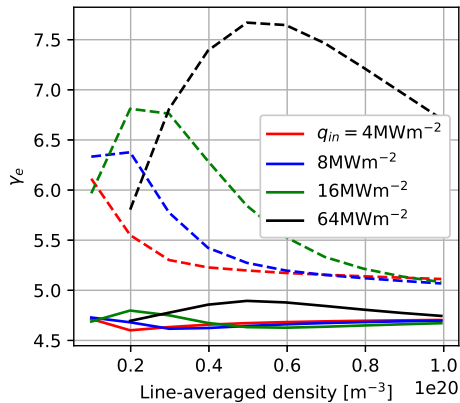


Figure 4: Electron energy distribution (isotropic part) close to the wall in a SOL-KiT simulation ($q_{in} = 64\text{MWm}^{-2}$, $\langle n \rangle = 5 \times 10^{19}\text{m}^{-3}$). Dashed line is the local Maxwellian. A prominent high-energy tail and thermalised bulk can both be seen. $T_e = 6.9\text{eV}$, $n_e = 3.1 \times 10^{20}\text{m}^{-3}$.

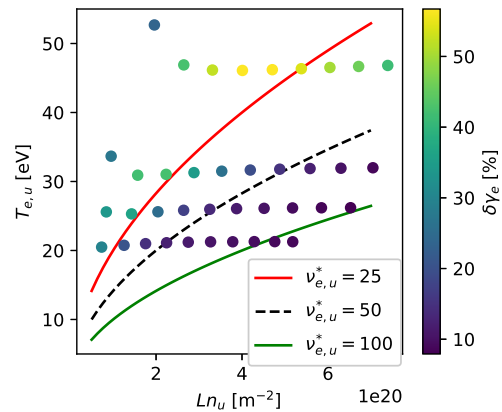
in kinetic mode, γ_e is calculated self-consistently from the logical boundary condition on the electron distribution, whereas in fluid mode it is calculated from fluid quantities (2). In Figure 5b, there are two regions where the kinetic and fluid calculations of γ_e are in good agreement, at both very low (top left) and very high (bottom right) collisionality. Similar behaviour was seen in a power scan in [12] and in a collisionality scan in [24]. The largest differences occur at low-intermediate collisionalities, but there is an additional increase in magnitude of this effect along lines of constant collisionality, moving towards larger $T_{e,u}$ and n_u . This can be seen by tracing along the red $\nu_{e,u}^* = 25$ line in Figure 5b, where simulations at higher $T_{e,u}$ have larger $\delta\gamma_e = (\gamma_e^{kinetic} - \gamma_e^{fluid})/\gamma_e^{fluid}$. Additionally, even at the highest collisionalities, where we would expect good agreement between fluid and kinetic predictions, there is a residual $\Delta\gamma_e = \gamma_e^{kinetic} - \gamma_e^{fluid} \simeq 0.5$. It would therefore appear that convergence of γ_e to the fluid value is slow as a function of collisionality.

Given the enhancement in γ_e for kinetic electrons, it is natural to investigate the heat lost to the sheath boundary, $q_{sh,e} = \gamma_e k T_{e,t} \Gamma_t$, where $T_{e,t}$ is the electron temperature at the target and Γ_t is the target particle flux. This is shown in Figure 6. In contrast to the kinetic enhancement in γ_e , we see that $q_{sh,e}$ is generally in good agreement for kinetic and fluid simulations. This is perhaps not surprising, since $q_{sh,e}$ is to a large extent fixed by q_{in} , as well as the fact that kinetic enhancement in γ_e may be offset by the reduction in target temperatures (Figure 3a). However, this does show that the overall power balance in these simulations (for example, how much power is radiated away by electron-neutral collisions) is broadly unchanged despite modifications to the conductive transport as well as behaviour at the boundary.

Finally, it is worth commenting that the findings in [12] and [5], that electron-neutral reaction rates are well-approximated by Maxwellian-averaged rates, is repli-



(a) Kinetic (dashed) and fluid (solid) values of γ_e , plotted for each density scan.



(b) $\delta\gamma_e = (\gamma_e^{kinetic} - \gamma_e^{fluid})/\gamma_e^{fluid}$ shown on the $T_{e,u}$ - Ln_u plane for each pair of fluid and kinetic simulations at a given q_{in} and $\langle n \rangle$.

Figure 5: Kinetic enhancement of γ_e , displayed two ways.

cated in this study. Differences in rate coefficients for deuterium ionisation and line radiation are negligible. Some differences in the total line-integrated particle source do exist in kinetic simulations (which takes into account ionisation and recombination as well as multi-step processes involving ex/de-excitation), but these are all under 10%, and are driven purely by differences in temperature profiles.

5 Discussion

The unchanged flux rollover behaviour in simulations with kinetic electrons (Figure 2), along with broadly similar heat loads to the walls (Figure 6), is indicative of the fact that a kinetic electron treatment does not significantly change the particle, momentum or power balance at equilibrium in this 1D SOL model. This is despite strong heat flux suppression (Figure 3) and enhancement of the sheath heat transmission factor (Figure 5). This can be understood as resulting from the fact that heat transport is primarily determined by the input power q_{in} . While a modified temperature profile is needed in kinetic mode to achieve the same parallel heat flux in these simulations, this is compensated by an enhanced γ_e which gives a similar $q_{sh,e}$, leaving the power balance broadly unchanged. In addition, differences in the temperature profile are insufficient to significantly change the particle source from electron-neutral interactions.

This power balance behaviour would not necessarily continue to be the case in the presence of strong radiation sinks from impurities, where modified temperature profiles and reaction rates could lead to differences in overall energy transport. This is the subject of an ongoing study.

The unchanged power balance despite the presence of kinetic effects in parallel heat flux and γ_e suggests that any attempt to capture kinetic effects in a fluid framework would need to consider both phenomena. As such, approaches which

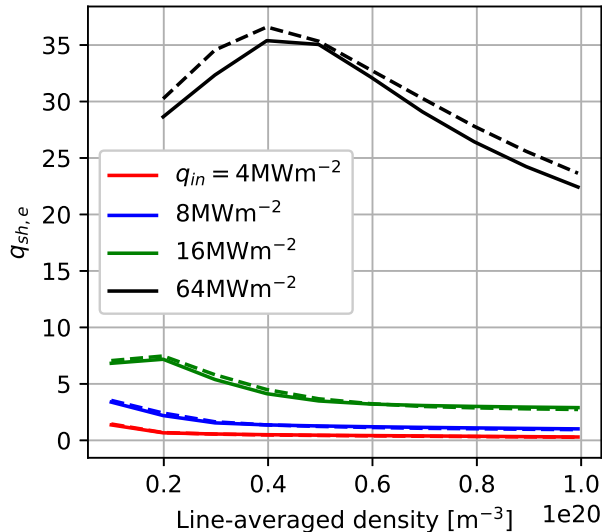


Figure 6: Sheath heat flux from electrons, $q_{sh,e}$ for kinetic (dashed) and fluid (solid) simulations.

treat only the modified heat flux [4] or the boundary condition [25] may not provide better predictive power than a purely fluid model.

The strong enhancements observed in γ_e are a result of the modified potential drop across the sheath when calculated kinetically, which is sensitive to electrons in the tail of the distribution. This may therefore have consequences for Langmuir probe measurements of the electron temperature in tokamak edge plasmas, as has been studied in [26]. Typically, an estimate is derived from an assumption of a Maxwellian electron distribution close to the sheath edge, but the characteristic distribution shown in Figure 4 may be more common. An attempt to quantify the change in γ_e is discussed in Section 6.

As discussed, and shown in [12] and [5], electron-impact ionisation rates of hydrogen are very well approximated by a Maxwellian distribution. This is unsurprising when considering the distribution shown in Figure 4, which is non-Maxwellian in the tail but very close to Maxwellian in the thermal bulk. Given the energy threshold of inelastic processes involving hydrogen are all at or lower than 13.6eV, the Maxwellian bulk electrons dominate the rates. This does suggest however that inelastic processes with threshold energies $\gtrsim 50\text{eV}$ (e.g. ionisation of high-Z impurities) may exhibit strong kinetic enhancement due to the presence of this enhanced tail. An ongoing study is currently investigating this.

A way of understanding the enhanced tail in the electron distribution close to the wall is as an ‘imprint’ of fast electrons from upstream, which have been transported downstream without having thermalised from collisions. This is seen clearly in Figure 7, where the upstream distribution is plotted alongside that close to the target. The gradient of the tail, related directly to the temperature on these axes, is the same in both cases. Therefore, if we assume the tail of the distribution at the target has temperature $T_{e,t}^{tail} = T_{e,u}$, then two conditions existing simultaneously produce a ‘strongly enhanced’ tail, which can lead to strong kinetic effects as discussed. These

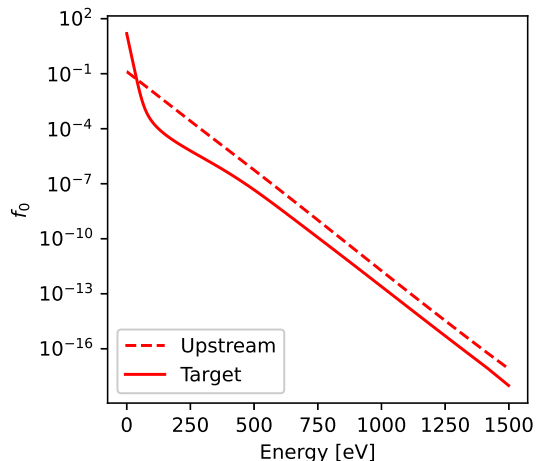


Figure 7: Electron energy distributions at two locations, upstream ($T_e = 40.3eV$) and close to the wall ($T_e = 6.9eV$). Electrons are close to Maxwellian upstream, and the fast tail survives to some extent further downstream.

are

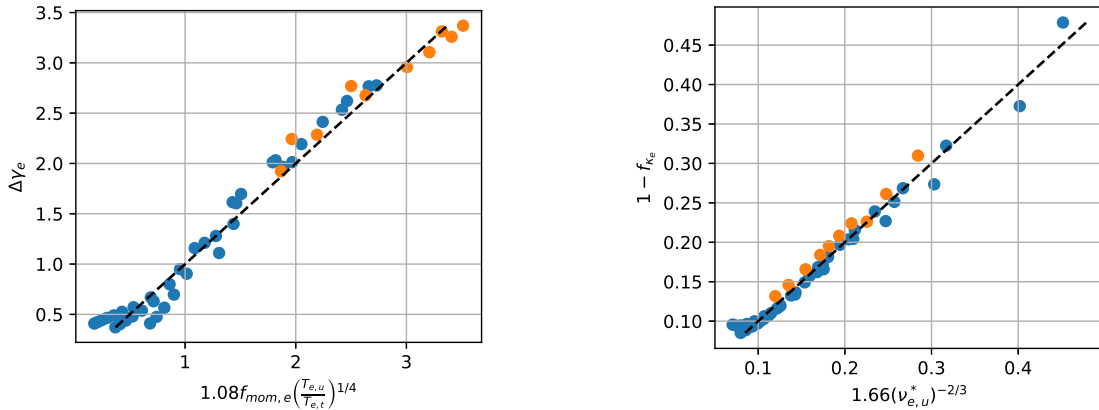
1. $T_{e,u} \gg T_{e,t}$,
2. small $\nu_{e,u}^*$.

In this study, we see that the imprint can survive up to moderate values of $\nu_{e,u}^*$ and hence drive kinetic effects, for example in the peak enhancement to γ_e occurring at $\nu_{e,u}^* \simeq 20$ (Figure 5). It is the interplay of upstream collisionality and parallel temperature drops which determines the strength of this imprint. For tokamak edge plasmas with large $T_{e,u}$ as well as significant power dissipation via impurities, we might expect both of these conditions to be satisfied.

Contrary to the heat flux suppression, which appears to be a monotonic function of $\nu_{e,u}^*$ as discussed in the next section, the enhancement to γ_e is more complex. It peaks at $\nu_{e,u}^* \simeq 20$, but also appears to increase for increasing $T_{e,u}$ at constant $\nu_{e,u}^*$. If this behaviour can be extrapolated to reactor-class devices then we may expect significant deviations from classical values of γ_e . This is discussed further in the next section.

6 Scaling relationships for observed kinetic effects

Any attempt at capturing kinetic effects at equilibrium in a fluid model of the scrape-off layer would appear to need to capture both modifications to the heat flux and enhancement to the sheath heat transmission coefficient. While models do exist for the former [27–29], they do not typically provide a self-consistent method for calculating modifications to the boundary behaviour. In [30], Tskhakaya et al. provide fits to the modifications to γ_e and parallel heat flux for the time-dependent response to a simulated edge-localised mode (ELM). Here, we present fits to the



(a) Kinetic modification to sheath heat transmission coefficient, γ_e .

(b) Line-averaged kinetic modification to heat conductivity, f_{κ_e} .

Figure 8: Proposed scalings for $\Delta\gamma_e$ and f_{κ_e} . Blue dots are the simulations carried out for this study, orange dots are from an additional density scan with different connection length and input power.

kinetic modifications to γ_e and $q_{\parallel,e}$ seen at equilibrium across a range of $T_{e,u}$ and n_u (and hence $\nu_{e,u}^*$), presented as functions of basic SOL parameters.

For the kinetic enhancement to γ_e , this is

$$\Delta\gamma_e = \gamma_e^{kinetic} - \gamma_e^{fluid} = 1.08 f_{mom,e} \left(\frac{T_{e,u}}{T_{e,t}} \right)^{1/4}, \quad (8)$$

where $f_{mom,e} = 2p_{e,t}/p_{e,u}$ is the electron momentum loss factor, related to the ratio of the electron pressure at the target to the pressure upstream. This is plotted against the simulation data in blue in Figure 8a. This has been used to predict the values of $\Delta\gamma_e$ in an additional density scan with $L = 30\text{m}$ and $q_{in} = 128\text{MWm}^{-2}$ (orange dots in Figure 8a). The agreement on the additional data is good, with an RMS error of 5.7%.

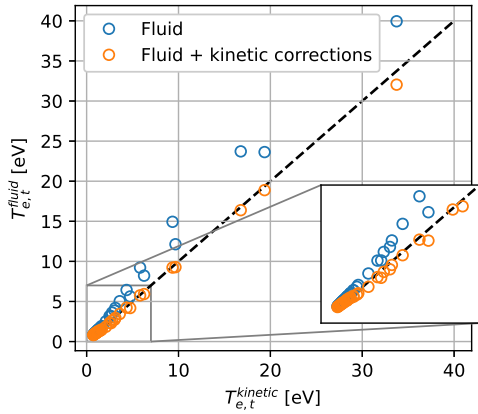
For the heat flux suppression, we first define a line-averaged modification to the heat conductivity, $f_{\kappa_e} = \frac{1}{L} \int q_{\parallel,e}^{kinetic} / q_{\parallel,e}^{SH} dx$. Figure 8b shows the fit to the relationship

$$1 - f_{\kappa_e} = 1.66 (\nu_{e,u}^*)^{-2/3}. \quad (9)$$

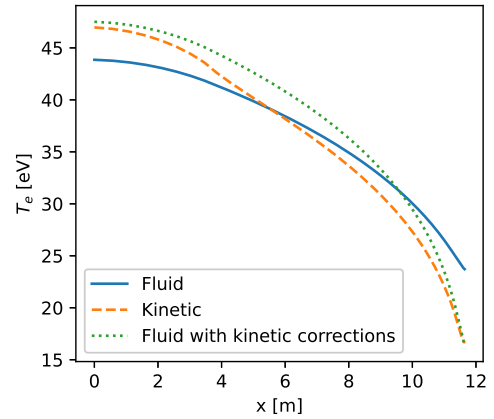
The RMS error on the additional runs is 6.9%.

The scaling for $\Delta\gamma_e$ predicts large kinetic effects for large values of f_{mom} (small momentum losses) and large values of $\frac{T_{e,u}}{T_{e,t}}$ (large temperature drops). Given that temperature drops along the SOL are facilitated in part by momentum losses [2, 20], these two effects will compete and we may expect a region of maximum enhancement to γ_e . The scaling for $1 - f_{\kappa_e}$ is a straightforward function of $\nu_{e,u}^*$, increasing at low collisionalities as expected.

The scalings presented here are straightforward to implement in a fluid model. Because of the spatial variation in heat flux suppression observed in these simulations (see Figure 3c), implementing the line-averaged quantity f_{κ_e} , for example as



(a) Target electron temperatures in kinetic simulations (x-axis) compared with fluid / fluid with kinetic corrections.



(b) Fluid, kinetic and fluid with kinetic corrections temperature profiles for $q_{in}=64\text{MWm}^{-2}$, $\langle n \rangle = 2 \times 10^{19}\text{m}^{-3}$.

Figure 9: Adding kinetic corrections to SOL-KiT fluid mode using equations (8) and (9).

a prefactor to the Spitzer-Härm conductivity, may not yield accurate temperature profiles but should be adequate for predicting the overall power balance. These scalings may also be used in simple analytical SOL models such as the modified two-point model [31] or the Lengyel model for predicting detachment onset with radiating impurities [32].

To test these relationships, we have implemented (8) and (9) in the fluid version of SOL-KiT, using self-consistent values of $f_{mom,e}$, $\frac{T_{e,u}}{T_{e,t}}$, etc. to calculate the modifications to $\gamma_e = \gamma_e^{fluid} + \Delta\gamma_e$ and $q_{||,e} = f_{\kappa_e} q_{||,e}^{SH}$. In Figure 9a, we compare the target temperatures in kinetic simulations with those in fluid simulations, with and without the kinetic corrections. Temperature profiles for a particular simulation are shown in Figure 9b. Agreement with $T_{e,t}$ is good, with the RMS error reduced from 26.0% to 7.1% with the addition of the kinetic corrections. Temperature profiles show that agreement is good at the upstream and target locations, but differences exist in the rest of the domain. This is expected due to the line-averaging of f_{κ_e} .

If we assume these scalings hold for larger values of $T_{e,u}$, n_u and L , then for the ITER scenario modelled in [33] (‘standard transport’ case; distance along the separatrix = 0cm), we would predict $\Delta\gamma_e = 1.95$ and $f_{\kappa_e} = 0.38$. For the DEMO tokamak scenario in [34], we get $\Delta\gamma_e = 4.28$ and $f_{\kappa_e} = 0.26$. It is possible that these regimes are beyond the validity of these scalings, which have larger $T_{e,u}$ than all the simulations in this study. In particular, the scaling for f_{κ_e} does not have the correct asymptotic behaviour for small $\nu_{e,u}^*$, which for $\nu_{e,u}^* < 2.14$, f_{κ_e} becomes negative.

A further caveat to (8) and (9) is that the plasma model in SOL-KiT does not currently include flux tube expansion (or other SOL geometry effects) or contributions from molecules or impurity species. The former will significantly alter parallel transport behaviour, and the latter will represent additional particle, momentum and energy sources/sinks. An ongoing project to redevelop SOL-KiT with a more flexible physics model, as well as improved computational efficiency and parallelisa-

tion, should make it possible to study kinetic effects in the presence of such additional physics.

7 Conclusion

We have presented kinetic studies of electron transport in tokamak scrape-off layer plasmas across a range of input powers and densities, under steady-state conditions.

One of the primary aims of this study has been to validate the local approximation in fluid models, which are frequently employed to model SOL plasmas. We see that, for SOL equilibria, a kinetic treatment of the electrons does not change qualitative behaviour in terms of the particle flux to the target with this plasma model, as shown in Figure 2, despite changes to the electron temperature profiles and reductions in the target temperatures (Figure 3).

Typically, it has been assumed that the classical value of γ_e is valid at equilibrium, but here there are differences of over 50%, as shown in Figure 5. We provide a qualitative understanding of this enhancement in terms of an imprint of the fast electrons from upstream on the electron distribution at the target. The presence of this enhanced tail is predicted to have significant impacts on collision rates for inelastic processes with threshold energies $\gtrsim 50\text{eV}$, for example the ionization of plasma impurities. This is the subject of an ongoing study.

The enhancement of γ_e and reduction in $q_{\parallel,e}$ at equilibrium is shown to follow simple scalings based on basic SOL parameters, (8) & (9). The performance of these fits is shown in Figure 8. To test the ability of these corrections to capture kinetic effects in SOL simulations, we have shown that implementing them in the fluid version of SOL-KiT does improve agreement with the fully kinetic T_e profiles. While there are caveats to the use of these scalings outside of SOL-KiT simulations, particularly in relation to the aspects of SOL physics not included in the model used here, it does suggest it is viable to capture kinetic effects at equilibrium in studies of future devices, either in fluid codes or reduced analytical models. Extrapolating to the ITER and DEMO tokamaks for example does predict relatively large kinetic effects in these devices, suggesting at least that further study into non-local parallel transport in reactor-class tokamaks is warranted.

The modifications to γ_e and $q_{\parallel,e}$ in conjunction with good agreement in power balance and target particle flux behaviour (discussed in Section 5 and shown in Figure 2), suggest that both effects contribute in a way which approximately cancels. As such, attempts to capture kinetic effects in fluid models should treat both phenomena simultaneously.

In this study, the changes to γ_e and $q_{\parallel,e}$ are in contrast to the behaviour at equilibrium found using the PIC code BIT1 in [35]. There, γ_e is found to be well-approximated by the classical value, and $q_{\parallel,e}$ is a non-monotonic function of collisionality, which is contradicted by (9). There are significant differences in the simulations carried out in [35], in particular that plasma-neutral interactions were neglected. In addition, only attached regimes were studied, limiting the possible values of the ratio $T_{e,u}/T_{e,t}$. Furthermore, the differences in γ_e seen here are of a similar magnitude to those seen with the KIPP code in [6].

It should also be noted that this investigation has been done for equilibrium

plasma conditions. For the sheath boundary condition in particular, much stronger kinetic effects may be present in transient regimes as shown in [3,35], albeit for short durations relative to inter-ELM equilibria.

Acknowledgements and supporting data

This work was funded by the UK Engineering and Physical Science Research Council (EPSRC) and the UK Atomic Energy Authority (UKAEA). It has also been improved through informal discussions with colleagues at UKAEA, in particular David Moulton.

The simulation data used in this study can be founds at <https://doi.org/10.14469/hpc/10979>.

References

- [1] S I Braginskii. Transport Processes in Plasmas. *Reviews of Plasma Physics*, pages 205–311, 1965.
- [2] P. C. Stangeby. The Plasma Boundary of Magnetic Fusion Devices. *Plasma Physics and Controlled Fusion*, 43(2):223–224, 2001.
- [3] S. Mijin, F. Militello, S. Newton, J. Omotani, and R. J. Kingham. Kinetic and fluid simulations of parallel electron transport during equilibria and transients in the scrape-off layer. *Plasma Physics and Controlled Fusion*, 62(9):095004, 2020.
- [4] M. Wigram, C. P. Ridgers, B. Dudson, J. P. Brodrick, and J. T. Omotani. Incorporating nonlocal parallel thermal transport in 1D ITER SOL modelling. 2020.
- [5] Menglong Zhao, A. V. Chankin, and D. P. Coster. Implementation of an inelastic collision operator into KIPP-SOLPS coupling and its effects on electron parallel transport in the scrape-off layer plasmas. *Contributions to Plasma Physics*, 59(7):1–13, 2019.
- [6] A. V. Chankin, G. Corrigan, and A. E. Jaervinen. Assessment of the strength of kinetic effects of parallel electron transport in the SOL and divertor of JET high radiative H-mode plasmas using EDGE2D-EIRENE and KIPP codes. *Plasma Physics and Controlled Fusion*, 60(11), 2018.
- [7] J. P. Brodrick, R. J. Kingham, M. M. Marinak, M. V. Patel, A. V. Chankin, J. T. Omotani, M. V. Umansky, D. Del Sorbo, B. Dudson, J. T. Parker, G. D. Kerbel, M. Sherlock, and C. P. Ridgers. Testing nonlocal models of electron thermal conduction for magnetic and inertial confinement fusion applications. *Physics of Plasmas*, 24(9), sep 2017.
- [8] D. Tskhakaya. Kinetic Modelling of the Detached Divertor Plasma. (633053), 2015.

- [9] J. T. Omotani and B. D. Dudson. Non-local approach to kinetic effects on parallel transport in fluid models of the scrape-off layer. *Plasma Physics and Controlled Fusion*, 55(5), 2013.
- [10] O. V. Batishchev, M. M. Shoucri, A. A. Batishcheva, and I. P. Shkarofsky. Fully kinetic simulation of coupled plasma and neutral particles in scrape-off layer plasmas of fusion devices. *Journal of Plasma Physics*, 61(2):347–364, 1999.
- [11] Z. Abou-Assaleh, M. Petravic, R. Vesey, J. P. Matte, and T. W. Johnston. Non-Local Transport in a Tokamak Plasma Divertor with Recycling. *Contributions to Plasma Physics*, 34(2-3):175–179, 1994.
- [12] S. Mijin, F. Militello, S. Newton, J. Omotani, and R. J. Kingham. Kinetic effects in parallel electron energy transport channels in the Scrape-Off Layer. Technical report, 2019.
- [13] D. Power, S. Mijin, F. Militello, and R. J. Kingham. Ion–electron energy transfer in kinetic and fluid modelling of the tokamak scrape-off layer. *The European Physical Journal Plus*, 136(11):1–13, 2021.
- [14] S. Mijin, A. Antony, F. Militello, and R. J. Kingham. SOL-KiT—Fully implicit code for kinetic simulation of parallel electron transport in the tokamak Scrape-Off Layer. *Computer Physics Communications*, 258:107600, 2021.
- [15] I. P. Shkarofsky, M. P. Bachynski, and T. W. Johnston. *The Particle Kinetics of Plasmas*. Reading, Mass.; Dordrecht printed, 1966.
- [16] Lyman Spitzer and Richard Härm. Transport phenomena in a completely ionized gas. *Physical Review*, 89(5):977–981, 1953.
- [17] R. K. Janev, D Reiter, and U Samm. *Collision Processes in Low-Temperature Hydrogen Plasmas*. 2003.
- [18] A. Kramida, Y. Ralchenko, and J. Reader. Nist atomic spectra database, 2020.
- [19] Richard J. Procassini and Dana A. Knoll. Kinetically motivated boundary conditions for fluid models of scrape-off layer transport. *Journal of Nuclear Materials*, 1992.
- [20] B. Dudson, J. Allen, T. Body, B. Chapman, C. Lau, L. Townley, D. Moulton, J. Harrison, and B. Lipschultz. The role of particle, energy and momentum losses in 1D simulations of divertor detachment. *Plasma Physics and Controlled Fusion*, 61(6), 2019.
- [21] N. Horsten, W. Dekeyser, G. Samaey, and M. Baelmans. Assessment of fluid neutral models for a detached ITER case. *Nuclear Materials and Energy*, 12:869–875, 2017.
- [22] P. Helander, S. I. Krasheninnikov, and P. J. Catto. Fluid equations for a partially ionized plasma. *Physics of Plasmas*, 1(10):3174–3180, 1994.

- [23] Michael R K Wigram. *Modelling tokamak power exhaust and scrape-off-layer thermal transport in high-power fusion devices*. PhD thesis, 2019.
- [24] M. Zhao, A. V. Chankin, and D. P. Coster. Kinetic simulations of electron heat flux in the scrape-off layer. *Nuclear Materials and Energy*, 12:819–824, 2017.
- [25] Ivona Vasileska and Leon Kos. Time-Dependent Boundary Conditions During ELMs in ITER Plasma. *Journal of Fusion Energy*, 39(5):212–220, 2020.
- [26] D. Tskhakaya, S. Jachmich, T. Eich, and W. Fundamenski. Interpretation of divertor Langmuir probe measurements during the ELMs at JET. *Journal of Nuclear Materials*, 415(1 SUPPL):S860–S864, 2011.
- [27] D. Del Sorbo, J. L. Feugeas, Ph Nicolaï, M. Olazabal-Loumé, B. Dubroca, S. Guisset, M. Touati, and V. Tikhonchuk. Reduced entropic model for studies of multidimensional nonlocal transport in high-energy-density plasmas. *Physics of Plasmas*, 22(8), 2015.
- [28] G. P. Schurtz, P. D. Nicolaï, and M. Busquet. A nonlocal electron conduction model for multidimensional radiation hydrodynamics codes. *Physics of Plasmas*, 7(10):4238–4249, 2000.
- [29] Jeong Young Ji, Eric D. Held, and Carl R. Sovinec. Moment approach to deriving parallel heat flow for general collisionality. *Physics of Plasmas*, 16(2), 2009.
- [30] D. Tskhakaya, F. Subba, X. Bonnin, D. P. Coster, W. Fundamenski, and R. A. Pitts. On kinetic effects during parallel transport in the SOL. *Contributions to Plasma Physics*, 48(1-3):89–93, 2008.
- [31] P. C. Stangeby. Basic physical processes and reduced models for plasma detachment. *Plasma Physics and Controlled Fusion*, 60(4), mar 2018.
- [32] L. Lengyel. Analysis of Radiating Plasma Boundary Layers. Technical report, IPP, 1981.
- [33] Irina Veselova, Elizaveta Kaveeva, Vladimir Rozhansky, Ilya Senichenkov, Anastasia Poletaeva, Richard A. Pitts, and Xavier Bonnin. SOLPS-ITER drift modelling of ITER burning plasmas with narrow near-SOL heat flux channels. *Nuclear Materials and Energy*, 26:100870, 2021.
- [34] Giulio Rubino, R. Ambrosino, G. Calabrò, V. Pericoli Ridolfini, and B. Viola. Comparative analysis of the SOL plasma in DEMO using EDGE2D/EIRENE and TECXY codes. *Nuclear Materials and Energy*, 12:864–868, 2017.
- [35] D. Tskhakaya, K. Matyash, R. Schneider, and F. Taccogna. The particle-in-cell method. *Contributions to Plasma Physics*, 47(8-9):563–594, 2007.